SCIREA Journal of Materials
http://www.scirea.org/journal/Materials
April 9, 2018
Volume 3, Issue 1, February 2018

Potentiostatic electrosynthesis of cerium conversion coatings on AA2024-T3 aircraft alloy in diammonium pentanitrocerate solutions

S. Kozhukharov[a*], Christian Girginov[b]

[a]Laboratory for Advanced Materials Research, University of Chemical Technology and Metallurgy, 8 Kl. Okhridsky blvd., 1756-Sofia, Bulgaria

[b] Department of Chemical Sciences, University of Chemical Technology and Metallurgy, 8 Kl. Okhridsky blvd., 1756-Sofia, Bulgaria

*stephko1980@abv.bg

Abstract

Cerium conversion coatings (CeCC) have been synthesized for corrosion protection of AA2024-T3 aircraft alloy through application of potentiostatic regime in aqueous solutions of diammonium pentanitrocerate - $(NH_4)_2Ce(NO_3)_5$. This cerium compound is used for first time for this purpose. The impact of the following deposition parameters: precursor solution concentration, the quantity of the H_2O_2 addition, the applied cathodic potential value, and the deposition duration on the deposition kinetics, the surface morphology, the microstructure, and the composition of the obtained coatings is investigated.

At the initial stage, the process is diffusion controlled, and subsequently it becomes be controlled by the CeCC nucleation and growth rate, following the island like growth mechanism, typical for this alloy. It has been established that the coatings obtained from 0,03 M $(NH_4)_2Ce(NO_3)_5$ solutions, with H_2O_2 addition in molar ratio between 2:1 and 4:1 in respect to Ce content, and applied potential E = – 1,0 V for 360 s possess uniform morphology and good adherence to the substrate. These optimal conditions are confirmed by quantitative evaluation of the coating roughness using Atomic Force Microscopy (AFM). The investigations, performed by Scanning Electron Microscopy (SEM), Energy Dispersion and Photoelectron Spectroscopy methods (EDS) and (XPS) reveal that the coatings possess net like structure (type «dry land»), being a mixture of Ce(III) and Ce(IV) oxides. The best coatings elaborated reach total Cerium content superior to 57 $\%_{wt}$, with Ce(IV) to Ce(III) relation equal to 85 : $15_{wt.}$ %.

Keywords: AA 2024-T3 Alloy; Rare earth elements; Electrodepositited films; AFM; SEM; XPS.

Introduction

The aluminium alloys are ranked second following the steels for industrial and household applications. Their mechanical properties – strength, stiffness and durability – combined with their low weight and relatively low price make them preferable constructive materials. For instance, about 70% of all metal details in the nowadays airplanes are composed of aluminium alloys [1]. Irrespective of their excellent mechanical properties, these alloys exhibit a serious disadvantage – they are susceptible to corrosion. It is attributed to the additive components (Cu, Fe, Mn, Mg, Si, etc.), which form intermetallics of a various composition dispersed throughout the aluminium matrix during the alloys hot rolling. In aggressive media, such as chloride ions containing one, these inclusions become centres of initiation and further proliferation of localised corrosion [2, 3]. During more than 50 years, the chromate conversion coatings were widely used as efficient corrosion protection of aluminium alloys as well as a large number of other alloys [4]. But the considerable toxicity and the carcinogenic effect imposed extremely restrictive regulations against the employment of Cr(VI) coatings [5, 6]. Various ions (MnO_4^-, MoO_4^-, WO_4^- and SiO_4^{2-}) containing, as well as solutions of borates, phosphates and nitrites were assessed as potential substitutions of the chromium compounds [7–10]. Hinton et al. [11-13] found that the rare-earth element containing substances, and particularly those containing cerium were reliable environmentally compatible alternative to Cr(VI) compounds for protection of aluminium alloys against corrosion. The authors proposed a method for deposition of cerium conversion coatings in cerium chloride solutions. The main disadvantage of the method was the remarkable time expense for the protective layer formation – about 90 hours. It was drastically reduced [14] by introduction of oxidisers (H_2O_2) to the cerium salt solution. This modified method was applied to protect a large number of aluminium alloys [15 - 20].

Hinton et al. proposed a new quick method for deposition of cerium conversion coatings, where the deposition is activated by cathodic current application [12]. This cathodic electrosynthesis was found appropriate for the protection of carbon steels [21 – 23], stainless steels [24 – 26, 28], steels galvanised by zinc [29 - 35], magnesium alloys [36], nickel [37, 38], etc.

Recently, successful formation of cerium conversion coatings on steel substrates was reported, through both spontaneous [39 - 41] and electrochemical [42] deposition methods. Furthermore, this type of coatings is also proposed for further enhancement of zinc-phosphate finishing of steel [43]. Another recent trend is the formation of combined, Ce-Ni [44] or Ce-V [45] conversion coatings on steel and magnesium alloys, revealing the versatility of this class of coatings and the possibilities to be combined with other elements and to be deposited on other metals and alloys. All these facts show that the methods used for cerium conversion coatings can be successfully applied for deposition on steel based materials and to be combined with other elements, like Ni, V, etc, in order to improve their corrosion protective properties and durability in real exploitation condition. But the number of aluminium alloys, used as substrates for cathodic electrosynthesis of cerium conversion coatings is relatively limited [46 – 50]. A single paper describing electrosynthesis at constant current in $CeCl_3$ solutions [51] is found in case of AA2014 alloy. The lack of experimental data regarding CeCC deposition on AA2024-T3 using electrolytes alternative to $CeCl_3$ as well as different regimes of electrosynthesis provoked the investigations reported in this paper. Aqueous solutions of $(NH_4)_2Ce(NO_3)_5$, a salt that has not been applied to CeCC deposition until nowadays on whatever substrate, is used in the experiments described. Furthermore, a potentiostatic regime is employed for coating electrosynthesis. This regime was initially tested by Hinton [11], while recently it was applied to deposition of cerium conversion coatings on A6060 alloy by using a solution mixture of $Ce(NO_3)_3$ and $NaNO_3$ [52]. Thus, the aim of the studies described is to synthesize cerium conversion coatings on AA2024-T3 alloy at constant cathodic potential using H_2O_2 containing solutions of $(NH_4)_2Ce(NO_3)_5$ and to evaluate the impact of the process parameters (the cerium salt concentration, the quantity of H_2O_2 additive, the applied potential value and the deposition duration) on the kinetics and mechanism of the process, as well as to perform detailed investigation of the superficial topology, microstructure and composition with the application of AFM, SEM, EDX, and XPS.

2. Experimental

The coating electrosynthesis was performed on AA2024-T3 copper-magnesium containing aircraft alloy delivered by "Southwest Aluminium group" (China). The exact composition of the alloy according to the producer's certificate is summarised in Table 1. Panels of this alloy with dimensions of 25mm x 25mm x 3mm underwent preliminary superficial treatment by alkaline etching in 50 g/l solution of NaOH for 2min at 50 ˚C, followed by acidic desmutting in diluted HNO_3 (the volume proportion in respect to the distilled water used was 1:1) for 5 min at room temperature. After each one of the procedures described above, the plates were submitted to vigorous washing with tap water for at least 2 min, followed by washing with distilled water.

Table 1. Standard and actual composition of the alloy investigated

Element	**Si**	**Fe**	**Cu**	**Mn**	**Mg**	**Cr**	**Zn**	**Ti**	**Al**
Standard content ($\%_{wt.}$)	≤ 0.60	≤0.50	3.90 4.90	0.30 0.90	1.20 1.90	≤0.10	0.25 0.09	0.15 0.02	Balance
Actual content ($\%_{wt.}$)	0.17	0.28	4.68	0.64	1.47	0.02	0.09	0.02	

A conventional three-electrode electrochemical flat cell, delivered by Metrohm, was used for the coating deposition. The preliminary treated metallic plates served as a cathode of exposed geometric area of 4 cm^2. The counter electrode was also a product of Metrohm. It was made of ss316 stainless steel, which passivated in the deposition solutions used. Ag,AgCl/3M KCl electrode (model 6.0733.100), a product of "Metrohm", served as a reference electrode. Diammonium pentanitrocerate solutions of concentrations of 0.01M, 0.03M and 0.10M containing H_2O_2 as an additive in 1:1, 2:1 and 4:1 molar proportion in respect to cerium were used for coatings deposition. The pH value of the solutions, which depended on the solution composition was not corrected. The electrosynthesis of the coatings was performed at cathodic potential values of –0.50 V, –1.00 V and –1.50 V versus the reference electrode. Potentiostat/Galvanostat “Autolab 30”, a product of Ecochemie (the Netherlands), was used. The current density transients during the coating deposition were recorded 5 s after the loading of the electrolyte to the cell. A Faraday cage protected the latter. All electrochemical procedures were carried out at room temperature in naturally aerated but not agitated solutions.

A square area of 49.5 μm side was used for the topographical observations performed by "EasyScan 2", a product of "Nanosurf" (Switzerland). The resolution was 256 points per line at an imaging rate of 2 seconds per line.

The SEM images were obtained using a scanning electron microscope TESCAN, SEM/FIB LYRA I XMU. The local composition was studied using energy dispersion X-ray spectroscopy, EDX (Quantax 200 of BRUKER detector) connected to the SEM-device.

The XPS studies were performed by Escalab MkII system (England) with Al K_α radiation (h = 1486.6 eV) and total instrumental resolution of ~1 eV. The pressure in the chamber was 1×10^{-8} Pa. The binding energy (BE) was referred to the C1s line (of the adventitious carbon) at 285.0 eV. The element concentrations were evaluated from the integrated peak areas after Shirley-type linear background subtraction using the theoretical Scofield’s photoionization cross-sections.

3. Results and discussion

3.1. Properties of H_2O_2 containing $(NH_4)_2Ce(NO_3)_5$ aqueous solutions

The aqueous solutions of diammonium pentanitrocerate exhibit some differences in their performance, when compared to those of other cerium salts. They have definitely acidic properties due to Ce-salt hydrolysis. The pH values of the pentanitrocerate solutions depend on their concentration (Table 2).

Table 2. pH values of $(NH_4)_2Ce(NO_3)_5$ solutions as a function of their composition

		Concentration of Ce-provider (M)		
Electrolyte condition	**Molar ratio H_2O_2: Ce**	0.01	0.03	0.1
Before H_2O_2 addition	----	3,30	2.70	2,05
After H_2O_2	2:1	3,25	2,71	2,06

addition	4:1	3,29	2,71	2.06
After coating	2:1	3,19	2,61	2,01
deposition	4:1	3,06	2,62	2.00

It is evident from the table that the pH values of the solutions used are in the pH range from 2.0 to 3.0, which is in fact optimal for spontaneous CeCC deposition [19]. That is why no additional correction of pH is required, unlike for instance $CeCl_3$ solutions, which have almost a neutral reaction. Furthermore, the pentanitrocerate solutions have a buffering ability due to the formation of a weak ammonium base obtained in the course of their hydrolysis. Table 2 shows that pH remains almost unchanged within H_2O_2 addition as well as coating electrosynthesis. This fact predetermines the significant stability of the deposition solutions in case of long-term storage and multiple deposition procedures.

Another advantage of the ammonium pentanitrocerate solutions is that they do not contain any aggressive Cl^- ions, so that stainless steel counter electrode can be used. The original "Metrohm" ss316 counter electrode used underwent passivation during anodic polarisation in these solutions. This is illustrated in Fig. 1 where the anodic polarization curves of a platinum electrode and ss316 electrode used are juxtaposed. Both curves are recorded in 0.03 M $(NH_4)_2Ce(NO_3)_5$ solution containing H_2O_2 additive in a molar proportion of H_2O_2:Ce = 2:1 at a potential sweep rate of 1 mV/s.

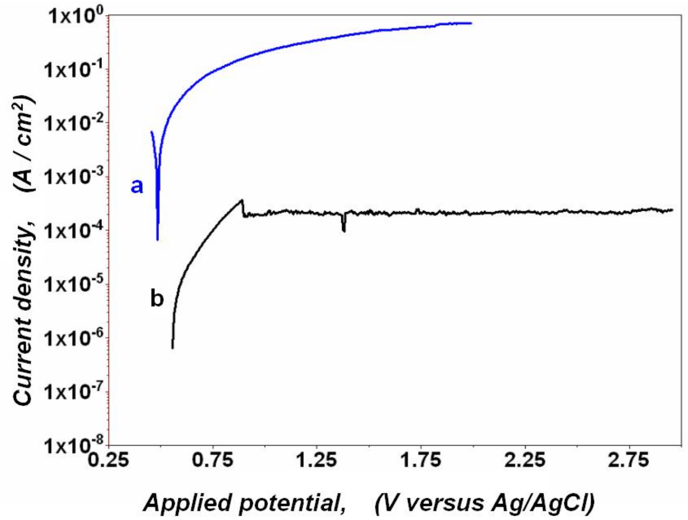

Fig. 1.Anodic polarization curves of a platinum electrode (a) and a commercial Metrohm electrode composed of ss316 (b), recorded in 0.03 M $(NH_4)_2Ce(NO_3)_5$ solution containing

H_2O_2 additive in a molar proportion of H_2O_2:Ce = 2:1 at a potential sweep rate of 1 mV/s.

The figure reveals that on anodic polarization the platinum electrode current density increases monotonically with the potential due to oxygen evolution (Reaction 1), while ss316 stainless steel electrode reaches a passive state, which stays independent of the potential.

No presence of chromium in the solutions or in the coatings is found on the ground of the atomic adsorption analysis, energy dispersion X-ray analysis and X-ray photoelectron spectroscopy.

3.2. Coatings formation mechanism and growth kinetics

The mechanism of CeCC electrosynthesis is widely discussed in the literature [22, 24 - 27, 37, 53 - 55]. It is considered that the initial stage refers to OH^- electrogeneration resulting from cathodic reactions proceeding in the electrolyte used. It is followed by interaction of the base generated on the working electrode surface with Ce^{3+} ions in the bulk of the solution. This results in precipitation of cerium oxides and hydroxides.

In fact aqueous solutions of three cerium salts have been so far used as source of Ce^{3+} ions, i.e. $CeCl_3$ [21, 38, 51], $Ce(NO_3)_3$ [22, 25, 37] and $Ce_3(SO_4)_2$ [26, 27]. Hydrogen peroxide has been always added to $CeCl_3$ solutions. It is assumed that in parallel with the oxygen cathodic reduction (Reaction 1),

$$O_2 + 2H_2O + 4e^- \rightarrow 4OH^- \qquad (1)$$

additional reduction of hydrogen peroxide takes place to give extra hydroxide ions (Reaction 2):

$$H_2O_2 + 2e^- \rightarrow 2OH^- \qquad (2)$$

In case of aqueous solutions of $Ce(NO_3)_3$ an addition of H_2O_2 is not necessary as hydoxide ions are obtained in the course of the dissolved oxygen reduction (Reaction 1) as well as nitrate ions reduction (Reaction 3) [22, 37, 52]:

$$NO_3^- + H_2O + 2e^- \rightarrow NO_2^- + 2OH^- \qquad (3)$$

Other parallel cathodic reactions can proceed depending on the solution pH leading to hydrogen evolution. They refer to hydronium ions and/or water reduction [22, 37].

The next stage in the conventional mechanism of CeCC cathodic electrosynthesis refers to the interaction of the base generated on the electrode surface with Ce^{3+} from the solution resulting in precipitation of cerium oxides/hydroxides. According to Aldykevich [57] the following reactions occur in this case. Ce^{3+} are oxidized to Ce^{4+} to form $Ce(OH)_2^{2+}$ (Reaction 4):

$$2Ce^{3+}_{aq.} + H_2O_2 + 2OH^- \rightarrow Ce(OH)_2^{2+}{}_{aq.} \qquad (4)$$

Because of the high OH^- content, the latter precipitate on the electrode surface in accordance with Reaction 5:

$$Ce(OH)_2^{2+}{}_{aq.} + 2OH^- \rightarrow Ce(OH)_4 \rightarrow CeO_2 + 2H_2O \qquad (5)$$

Direct interaction of Ce^{3+} and OH^- ions is also possible (Reaction 6). It leads to the precipitation of $Ce(OH)_3$:

$$Ce^{3+} + 3OH^- \rightarrow Ce(OH)_3 \qquad (6)$$

The further electrochemical oxidation of $Ce(OH)_3$ to cerium CeO_2 can also proceed in the course of the spontaneous coating deposition (Reaction 7):

$$Ce(OH)_3 \rightarrow CeO_2 + H_3O^+ + e^- \qquad (7)$$

This in fact conventional mechanism of CeCC electrosynthesis is not valid in case of diammonium pentanitrocerate. Because of the presence of NO_3^- ions, these solutions can be used in absence of H_2O_2 (see Reaction 3). But the experiments carried out in the course of the present investigation showed that any coating deposition by cathodic polarization in diammonium pentanitrocerate solutions requires H_2O_2 addition. This provides the assumption that the nitrate ions in $Ce(NO_3)_5^{2-}$ are bonded in a relatively stable complex anion, which hinders the occurrence of Reaction 3.

The base electrogeneration can occur only after addition of H_2O_2 to the solution as in the case of $CeCl_3$ solutions. It is supposed that the peroxide introduced becomes the basic source of hydroxide ions in accordance with Reaction 2. The latter occurrence is accepted without any critical analysis according to us in most of the publications referring to spontaneous and electrochemical deposition of cerium conversion coatings. The proceeding of such reaction is however doubtful because the peroxide is always present in the form of an aqueous solution and the water ions effect cannot be ignored. This complicating interaction can most probably explain the lack of any data referring to the standard electrode potential of Reaction 2. The detailed description of all possible equilibria in the system Ce(III)/Ce(IV) – H_2O – H_2O_2/O_2 [58] presented to accomplish cerium Pourbaix diagram does not mention Reaction 2. But it points out that the thermodynamically possible cathodic reaction of hydrogen peroxide in water solutions is described by Reaction 9:

$$H_2O_2 + 2H^+ + 2e^- \rightarrow 2H_2O, \quad E^0 = 1.776\ \text{V/SHE [59]} \qquad (9)$$

Hence water but not hydroxide ions is produced. A question arises then. As the peroxide reduction cannot proceed without water ions participation and besides no base can be obtained in the course of Reaction 2, is there any other mechanism of peroxide reduction to hydroxide ions? According to us there is such a possibility in view of concepts developed by Scholes et al. [60]. They accept that Ce^{3+} ions in the solution react with the molecules of hydrogen peroxide added forming polynuclear cerium peroxo-compelexes (Reaction 10):

$$Ce^{3+}_{aq.} + H_2O_{2aq.} \rightarrow Ce(H_2O_2)_{aq.}^{3+} \qquad (10)$$

This reaction is slow and time is required for the establishment of equilibrium between Ce^{3+}, the hydrogen peroxide added and the peroxo-complexes $Ce(H_2O_2)_{aq.}^{3+}$. At electrode cathodic polarization this equilibrium will be shifted because of the proceeding of Reaction 11:

$$Ce(H_2O_2)_{aq.}^{3+} + 2e- \rightarrow Ce^{3+}_{aq.} + 2OH^- \qquad (11)$$

The latter is much more probable than Reaction 2 because the peroxide bond (O–O) in hydrogen peroxide molecules within the cerium peroxio-complexes is weakened when compared to that in hyrogen peroxide molecules in the bulk of the solution. Hence, it could be assumed that Ce^{3+} ions catalyze in fact the reduction of H_2O_2 to OH^-.

Thus, the slow chemical Reaction 10 foreruns the formation of hydroxide ions on the electrode surface. Its kinetics affects all subsequent electrochemical reactions related to CeCC deposition. It can be treated as a rate-determining step of the overall process of coating electrosynthesis. The pathway described is further complicated due to the fact that the superficial concentration of cerium peroxo-complexes will differ from that in the bulk of the solution within Reaction 10 timespan leading thus to a concentration gradient in the electrode vicinity. This gradient will promote a transport of cerium peroxo-complexes towards the electrode by diffusion predetermining thus diffusion current appearance. Two extreme cases can be outlined under these conditions. The first one refers to a rate of the chemical reaction lower than that of the substance transport. This leads to electrosynthesis of cerium conversion coatings proceeding as an electrochemical process forerun by a homogeneous chemical reaction. The second case is observed when the peroxo-complex transport is slower than the forerunning chemical reaction. In this case a nonstationary initial diffusion current can be detected. In fact such current is experimentally observed (see Fig. 2 and the related comments).

The base formation on the electrode surface depends predominantly on the electrolyte composition. The coatings growth kinetics, however, their structure and composition are basically predetermined by the substrate nature and surface state.

AA2024-T3 aircraft alloy has remarkable non-homogeneity due to the alloying elements, which form during the hot rolling. The obtained individual intermetallic particles of various compositions are dispersed throughout the bulk of the aluminium matrix. The most widely spread are Al_2(Cu, Mg) particles [2], followed by those of Al_{16}(CuFeMn) composition [3]. Besides, the alloy contains a large number of dispersoide particles of a size of ca 10nm – 100nm, as well as precipitates formed during the thermal treatment [56]. The preliminary alkaline treatment accepted as a practice in the present investigation does not affect the alloy's surface heterogeneity. It leads to the formation of a gel layer of aluminium hydroxides, which is conductive and enables the proceeding of Faraday's reactions [19]. It is not distributed uniformly on the entire metal surface. It is thinner and contains more defects at the intermetallic particles areas [49]. Under cathodic polarisation conditions Reactions 1–5 start earlier there. This provides the formation of island-like discrete precipitates of cerium oxides/hydroxides. Such a surface is shown in Fig. 5 (section 3.4). At further cathodic polarisation other areas of lower cathodic activity start to involve in the electrosynthesis process. The passive film formed during the preliminary alkaline treatment dissolves to be further substituted by cerium oxides/hydroxides precipitates [19, 56]. This "island growth" mechanism [61, 62] is confirmed by the SEM images presented in Fig. 5 (section 3.4).

The mechanism described influences the film growth kinetics, which can be illustrated by the shape of the current transients. Fig. 2 shows such a transient recorded during coating deposition at E = -1.0 V in 0.03 M $(NH_4)_2Ce(NO_3)_5$ with H_2O_2 additive in a molar ratio of 2:1 in respect to cerium.

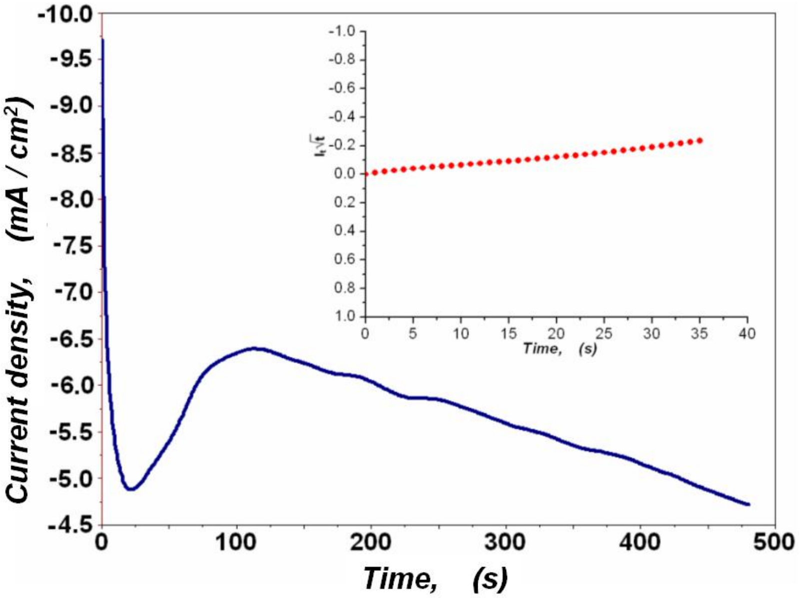

Fig. 2. Current transient recorded during CeCC deposition at E = -1.0 V in 0.03 M $(NH_4)_2Ce(NO_3)_5$ solution containing H_2O_2 additive in a molar proportion to Cerium of 2:1.

The transient is characterized by a well outlined initial minimum followed by a broad peak and subsequent monotonous current decrease. Unlike the case described in ref. [52], the currents recording in the present investigation starts almost immediately (5 s) after the contact of the electrode with the solution, i.e. without 15 min waiting to reach a stationary OCP. The latter time delay could result in a spontaneous coating deposition on the most active sites on the electrode surface masking thus the initial coating growth.

Fig. 2 shows that the absolute value of the cathodic current decreases sharply at the very beginning. Other authors observed no such current decrease. It can be demonstrated that this non-stationary current is of diffusion nature and hence can be described by the Cottrell's equation [63]:

$$I_t = i_d A = \frac{nFc^0\sqrt{D}}{\sqrt{\pi t}} A \qquad (12)$$

where I_t is the current value measured at a given moment, i_d is the diffusion current density, A is the electrode surface area, n is the number of electrons exchanged in the reaction, F is the Faraday constant, t is time, while c^0 and D are the initial bulk concentration and the diffusion coefficient of the diffusing agent, respectively.

It follows from this equation that the product $I_t\sqrt{t}$ should be a constant if A is the geometric surface area of the electrode staying constant with time. It follows then that the dependence $I_t\sqrt{t}$ vs. time should be a straight line running in parallel to the abscissa. This behavior is illustrated by the inset of Fig. 2. It is worth noting that the straight line presented has a slope different from zero. This can be most probably attributed to the dissolution of the passive film formed during the preliminary alkaline treatment. Bard and Faulkner [63] analyze the factors that influence the Cottrell's diffusion current and come to the conclusion that the available "time window" of Cottrell's measurements lies approximately between 20 μs and 200 s. Fig. 2 shows that the time required for the diffusion current recording under our experimental conditions is ca 25 s. The latter value is in full correspondence with these constrains.

Hence it follows that the process of CeCC electrosynthesis on AA2024-T3 is initially diffusion controlled. However, it alters its character in the course of deposition. In accord with the island-like coating growth considerations the active working area θ expands because of the permanent involvement of new less active cathodic zones thus predetermining the increase of the current recorded at a fixed potential value. This can possibly explain the current increase following the minimum of the current transient. This trend will continue until a notable resistance by the deposits [37] starts to act, which in turn will bring a monotonic current decrease. Hence, the initial minimum observed in the current transients of AA2024 alloy is determined by the proceeding of a non-stationary diffusion current and subsequent expansion of the active working surface area of the electrode caused by the island-like coating growth.

This mechanism is valid for each of the zones of the electrode surface because of the extremely heterogeneous surface of AA2024-T3. This implies that areas of nucleation will simultaneously exist with zones of growth of already formed nuclei. The SEM images in section 3.3 reveal discrete areas of different rates of coverage deposition. It is noteworthy to mention that the coatings do not block completely the metal surface, so that considerable electrical conductivity is still observed. The latter is discussed in section 3.4.

3.3. Impact of the deposition parameters on the appearance and the superficial morphology of the coatings

Fig. 3 illustrates the dependence of the deposit growth on the concentration of the deposition solution, the applied potential and the quantity of H_2O_2 introduced.

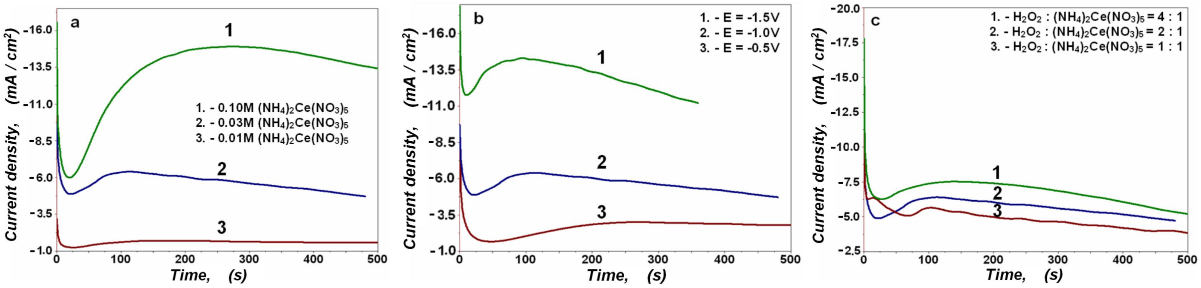

Fig. 3. Current transients obtained as a function of $(NH_4)_2Ce(NO_3)_5$ solutions concentrations (a), deposition potential values (b), and H_2O_2 amounts added (c).

The figure above shows that currents increase with (i) the increase of the salt concentration; (ii) the shift of the potential to more negative values and (iii) the increase of hydrogen peroxide amount. These are the factors, which promote the film growth acceleration. In fact the film growth affects significantly the outlook of the coatings obtained and their adhesion to the substrate. The moderate deposition growth (i.e. lower deposition rate) provides to obtain gold-like films with a good adherence to the substrate. The latter was verified by adhesive tape-tests. The higher rates of electrosynthesis refer to the formation of dark-reddish coatings that can easily be removed from the substrate surface by washing with water. This means that the conversion coatings deposited at a higher rate do not completely insulate the substrate surface, but provide some electrical conductivity, so that new Ce-oxides/hydroxides of inferior adhesion ability continue to form. A brighter layer covering unevenly the substrate is observed upon this type of coatings removal. It has to be noted that the deposition time required to obtain relatively good coatings depends on the combination of all three parameters – the Ce-concentration, the cathodic potential, and the amount of hydrogen peroxide introduced. It is found that good coatings can be obtained at E = - 1.0 V in 0.03 M $(NH_4)_2Ce(NO_3)_5$ solutions with the addition of H_2O_2 in molar proportions to cerium in the range from 2:1 to 4:1 and deposition time within the range from 360 s to 480 s.

AFM was used for qualitative and quantitative characterisation of the coatings' superficial morphology. The coating obtained at the optimal conditions (i.e. 0.03 M $(NH_4)_2Ce(NO_3)_5$ solution with H_2O_2 introduced in a molar ratio to Ce of 2:1 at deposition potential of -1.0 V) was compared to two coatings deposited under identical deposition parameters but in solutions of varying Ce salt concentrations: 0.01M and 0.10 M. The results are shown in Fig. 4:

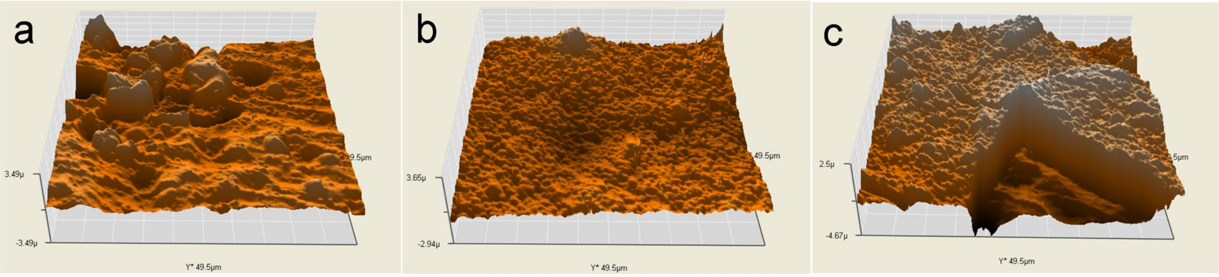

Fig. 4. AFM images of the topography of coatings deposited at E = -1.0 V in diammonium pentanitrocerate solutions of different concentrations: a- 0.01M; b- 0.03M, and c- 0.10M and a molar ratio of H_2O_2 to Ce of 2:1

Fig. 4 indicates that the coatings obtained in solutions of low Ce-salt concentration (i.e. 0.01 M) are discrete, non-uniform, island-like deposits. Wide areas of bare metal surface are left unchanged. Unlike them, the coatings deposited under the optimal conditions cover completely the electrode surface. They have fine-grained structure. Rare island-like deposits are observed. The conversion coatings deposited in concentrated solutions (0.10 M) have a complex structure. They are composed of a thick outer granular layer, which is randomly detached, and an underlayer containing a net of ruptures. The following parameters were used for the quantitative coating topology evaluation: the highest peak height (S_p), the depth of the deepest valley (S_x), both measured with reference to the base plane, the difference between Sp and Sv (S_y), and the mean roughness value (S_m). The values obtained are summarized in Table 3.

Table 3. Values of the roughness parameters characterizing the superficial morphology of coatings obtained in pentanitrocerate solutions of different concentrations

Roughness parameter	**Solution Concentration (M)**		
	0.01	**0.03**	**0.10**
Sp, (nm)	3100	2500	3077
Sv, (nm)	-2670	-1400	-5500
Sy, (µm)	5.77	3.94	8.57
Sm, (pm)	-1.95	3.16	99.00

The results in Table 3 confirm quantitatively the differences in the topology of the specimens studied as shown in Fig. 4. The smoothest coating of Sm = 3.16 pm is obtained in 0.03M $(NH_4)_2Ce(NO_3)_5$ solution, whereas the roughest one of Sm = 99.00 pm is obtained in 0.10 M solution. The coatings obtained at potentials different from E = -1.0 V have inferior characteristics and they are not shown in this paper.

3.4. Microstructure and elemental composition

Fig. 5 presents a series of SEM images acquired at low (1500x) and high (5000x in the insets) magnification of coatings obtained at E=-1.0 V in 0.03 M solutions of $(NH_4)_2Ce(NO_3)_5$ with H_2O_2 presence in a molar ratio of H_2O_2:Ce=2:1 and different deposition times.

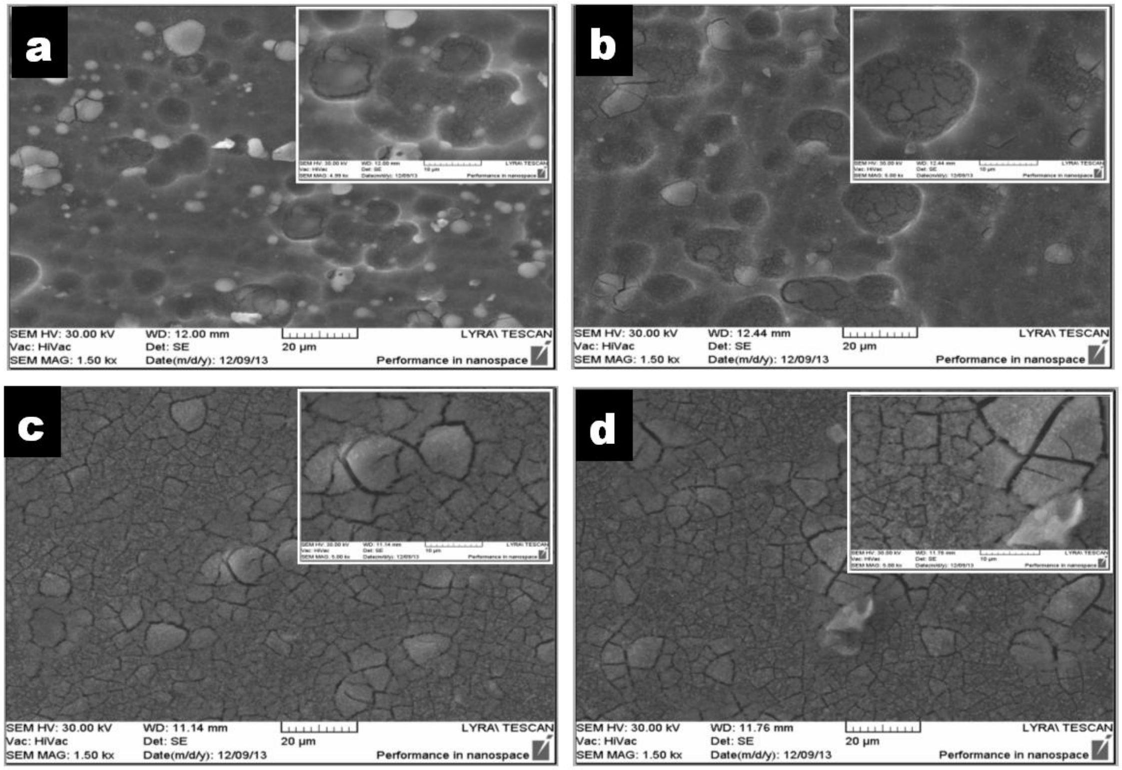

Fig. 5. SEM images of CeCC deposited at E=-1.0 V in 0.03 M $(NH_4)Ce(NO_3)_5$ solutions with the addition of H_2O_2 in a molar proportion of H_2O_2:Ce =2:1 and different deposition times: (a) - 120 s; (b) - 240 s; (c) - 360 s; (d) - 480 s

Discrete islands of cerium hydroxides/oxides are formed during the initial 120 s (Fig. 5a) of deposition. They are deposited on the most cathodically active intermetallics where the passive film has the lowest thickness and the highest number of defects [48]. Crevices start to appear simultaneously with the island-like deposits formation. This effect is attributed to the dissolution of the passive film. Nets of cracks start to outline at the bottom of these crevices. They reveal the presence of ceria deposits (Fig.5b). The latter changes are observed until the 240-th second. After 360 s of electrodeposition the entire surface of the specimen is already covered by ceria film (Fig. 5c). Its density increases within the following 120 s (Fig. 5d). The film obtained includes dense, strongly ruptured island-like deposits of cerium hydroxides/oxides surrounded by a net of cracks alluding thus “dry land”.

Fig. 6 outlines the effect of the deposition duration on the microstructure of CeCC, deposited in 0.10 M solution. It is evident that in case of a high concentration of the deposition solution the microstructural changes proceed much more rapidly. The island-like deposits observed at the

120th second convert entirely to a strongly cracked layer. This fact reveals that the coatings do not block completely the substrate surface, but provide some electrical conductivity.

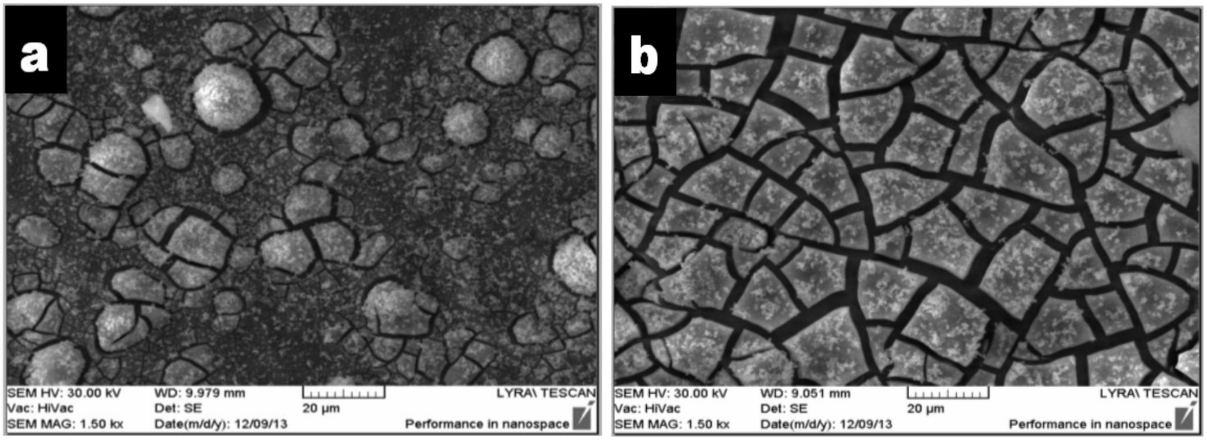

Fig. 6. SEM images of coatings deposited at E=-1.0 V in 0.1 M solutions of diammonium pentanitrocerate doped by hydrogen peroxide in molar ratio of H_2O_2:Ce = 2:1 at deposition time of (a) 120 s; (b) 240 s

The EDX analysis reveals that the composition of the film depends on the substrate superficial morphology. Fig. 7 shows the composition of the coating obtained at E=-1.0 V within 360 s in 0.03 M diammonium pentanitrocerate solution doped by hydrogen peroxide in molar ratio of H_2O_2:Ce = 2:1. A great difference of the local composition is registered for the zone of highest density (point 2) and these of lower density (points 1 and 3). The cerium content at point 2 is 54.57 wt. %, while it is 31.24 wt. % at the other points.

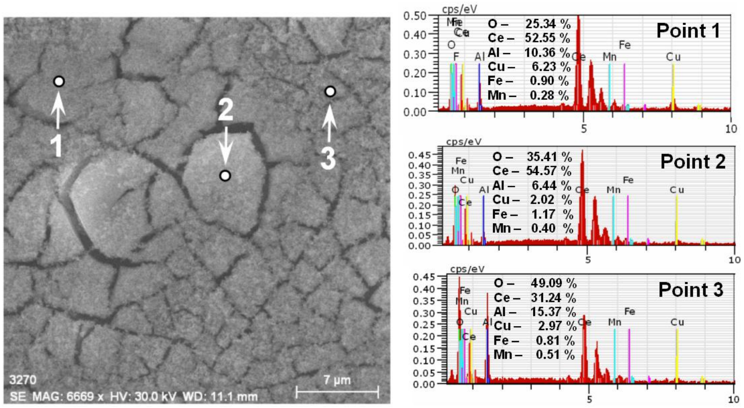

Fig. 7. EDX point analyses of CeCC electrodeposited for 360 s at E=-1.0 V in 0.03 M diammonium pentanitrocerate solutions doped by hydrogen peroxide in molar ratio of H_2O_2:Ce = 2:1

The composition of the film undergoes changes during the electrodeposition. The Ce-content increases. Fig. 8 reveals the composition of a coating obtained after 480 s of electrosynthesis.

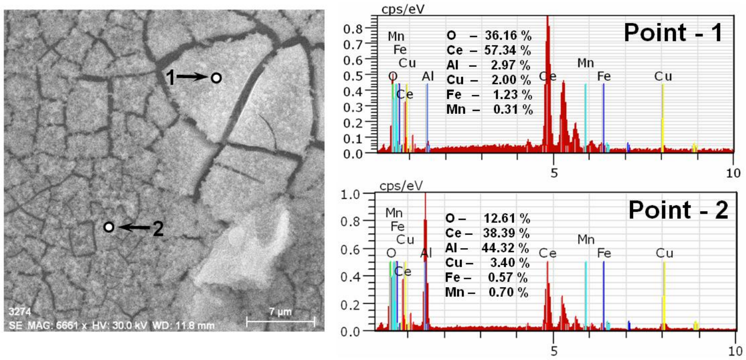

Fig. 8. EDX analyses of CeCC electrodeposited for 480 s at E=-1.0 V in 0.03 M of diammonium pentanitrocerate solutions doped by hydrogen peroxide in molar ratio of H_2O_2:Ce = 2:1

The juxtaposition of Figs. 7 and 8 reveals that Ce amount in the coating deposited for 480 s is higher than that of the coating deposited for 360 s. Its content increases from 55.57 % (Fig. 7, point 2) to 57.34% (Fig. 8, point 1) at the zones of higher density, whereas at the other zones it increases from 31.24% (Fig. 7, point 3) to 38.39 %, (Fig. 8, point 2), respectively. This fact is rather interesting. It shows that the cerium hydroxide/oxide coatings possess some electrical conductivity and do not insulate completely the surface of the sample. Whether this conductivity is electronic [37] or it originates from ionic vacancies in the oxide film is a problem that is not discussed in this paper. It is rather probable that the electrical conductivity determined by the electrolyte penetrating the coating's pores is of an ionic character.

It is evident from the EDX data that small quantities of Ce (2% - 9%) are present at the cracks bottom (not shown in the figures). This fact shows that the ruptures are not formed only during the drying, i.e. they are not only attributed to the coating shrinkage. They appear even during the coating electrosynthesis because of the stress between the coating and the underlying substrate.

All investigations aimed at the determination of the real composition of the CeCCs reveal that, in general, they are miscellaneous mixtures composed of Ce(III)/Ce(IV) oxides/hydroxides. It is assumed that the oxides/hydroxides of cerium in its fourth oxidation stage have superior protective ability [2, 64] due to the extremely low solubility of these compounds in water [65]. The present paper reports data obtained by XPS on Ce(III)/Ce(IV) proportion in view of the total

Ce-content. For this purpose, three specimens denoted as P1, P2, and P3 of visually uniform coverage (see Table 4) were submitted to analysis. The obtained detailed spectra of Ce3d$_{5/2}$ and Ce3d$_{3/2}$ are shown in Fig 9.

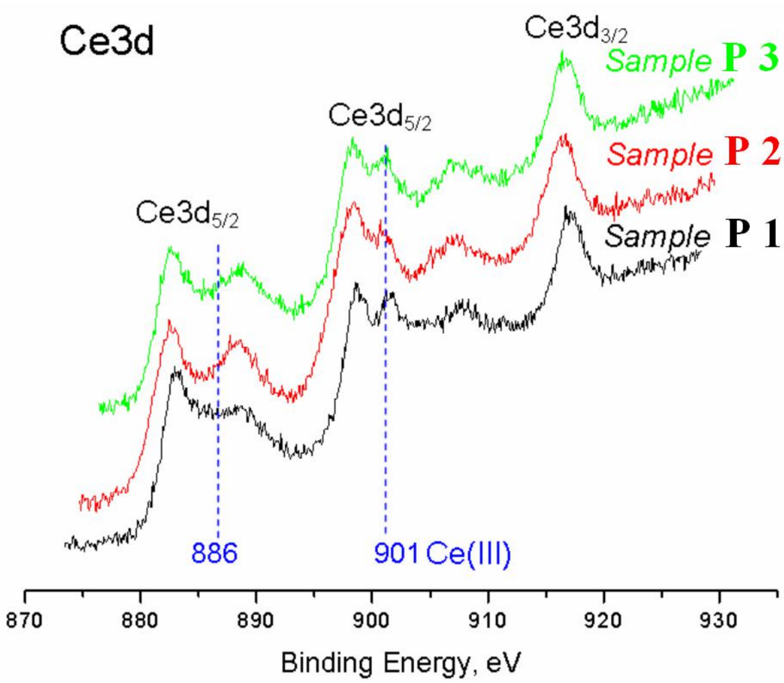

Fig. 9 XPS Ce3d partial spectra of samples P1, P2 and P3

It is seen that there are peaks identifying Ce3d$_{5/2}$ (882,3 and 898.3 eV) and Ce3d$_{3/2}$ (916.7 eV), respectively. They are indicative for the presence of Ce(IV) oxidation state [64]. The peaks at 886eV, 903.9eV and 907,1eV could be assigned to a contribution from Ce(III) oxidation state. The presence of a satellite peak at 917eV is a supplemental confirmation for the formation of Ce(IV) species according to Hoang [66]. The spectra in Fig 9 were submitted to a quantitative analysis aiming to determine the proportion between Ce(III) and Ce(IV) compounds. The data obtained are summarised in Table 4.

Table 4. Data obtained by quantitative analysis of the XPS spectra obtained

Sample	Deposition conditions*			Content ($\%_{wt.}$)
	$(NH_4)_2Ce(NO_3)_5$	Applied	Duration	

	concentration (M)	potential (V)	(s)	Ce(III)	Ce(IV)
P1	0,03	E = -1.5 V	120	20.9	79.1
P2	0,03	E = -1.0 V	360	15.0	85.0
P3	0,10	E = -1.0 V	60	6.0	94.0

Table 4 reveals that Ce(IV) content is significant for all specimens investigated being in the range from 80 wt. % to 94 wt. %. This predetermines the coatings high capability to provide protection of AA2024-T3 alloy. The impact of ss 316-counter electrode on the coating composition was followed as well. A XPS spectrum was recorded in the range from 0eV to 1300eV (it is not shown in the figures). The absence of Cr 2p peaks at 577 eV and 586 eV verifies the absence of any contamination of the coatings by chromium from the stainless steel counter electrode.

Conclusions

The investigation presented focuses on the characterization of the superficial morphology, microstructure and composition of cerium conversion coatings deposited on AA2024-T3 at a constant cathodic potential in $(NH_4)_2Ce(NO_3)_5$ aqueous solutions doped with H_2O_2. The deposition mechanism and the film growth kinetics are clarified on the basis of the experimental data obtained.

The advantages of $(NH_4)_2Ce(NO_3)_5$ are outlined in comparison to other sources of cerium described in the literature so far. The diammonium pentanitrocerate solutions do not require supplemental pH correction. Furthermore, because of their buffering ability, these solutions preserve their initial pH values (predetermined by their concentration) for extended storage periods and multiple deposition procedures.

On the basis of the coatings outlook, their adherence to the substrate and superficial morphology, assessed qualitatively and quantitatively by means of AFM, the coating deposition conditions are optimized so that gold-like, uniform, and adherent layers are obtained. Such coatings are deposited for 360 s at a cathodic potential of E= - 1.0 V in 0.03 M diammonium pentanitrocerate solutions doped with H_2O_2 in a molar ratio with regard to cerium content of 2:1 to 4:1. Coating layers deposited in more concentrated solutions have a good outlook and coverage but unsatisfactory adhesion to the substrate.

The possible mechanism of the cathodic potentiostatic CeCC electrosynthesis using $(NH_4)_2Ce(NO_3)_5$ solutions is also discussed taking into specific consideration H_2O_2 reduction. The conventional concept assuming direct peroxide reduction with no water ions participation is found inadequate. An alternative mechanism validating the cerium ions catalytic role in this process is advanced.

Current transients revealing the evolution of the cathodic current with time at a constant potential value are recorded varying the electrosynthesis parameters. The analysis of the transients shows that the process of coating electrosynthesis is initially diffusion controlled. It is subsequently determined by the crystal growth rate in accord with the “island-like deposition” model.

The coatings mictrostructure is characterized by SEM and EDX analyses. The elemental composition of CeCC deposited under optimal conditions is determined. It is demonstrated that the coatings consist of island-like domains surrounded by nets of cracks. The cerium content can reach 57,30 wt. % depending on the deposition conditions applied. It is only in the range from 2% to 9% at the cracks bottom.

The XPS analysis reveals that the CeCC synthesized at constant potential are composed of miscellaneous mixtures of Ce(III) and Ce(IV) compounds with Ce(IV) predominance. The latter varies between 80% and 94% depending on the synthesis conditions. In accord with the literature data this composition provides the assumption that CeCC can efficiently protect AA2024-T3 aircraft alloy against corrosion.

Acknowledgements: The authors gratefully acknowledge the financial support provided by National Scientific Fund of Bulgaria, **Project DM 19/6**

References:

[1] L. E. M. Palomino, I. V. Aoki, H. G. de Melo, Microstructural and electrochemical characterization of Ce conversion layers formed on Al alloy 2024-T3 covered with Cu-rich smut, Electrochim Acta, 5 (2006) 5943–5953.

[2] K. A. Yasakau, M. L. Zheludkevich, S. V. Lamaka, M. G. S. Ferreira, Mechanism of corrosion inhibition of AA2024 by rare-earth compounds, J. Phys. Chem. B, 110 (2006) 5515-5528

[3] M. Bethencourt, F. J. Botana, M. J. Cano, M. Marcos, J. M. Sánchez-Amaya, L. González-Rovira, Behaviour of the alloy AA2017 in aqueous solutions of NaCl. Part I: Corrosion mechanisms, Corros. Sci. 51 (2009) 518-524.

[4] M. Bethencourt, F. J. Botana, J. J. Calvino, M. Marcos, M. A. Rodriguez-Chacon, Lanthanide compounds as environmentally-friendly corrosion inhibitors of aluminium alloys: a review, Corros. Sci. 40 (1998) 1803-1819.

[5] Directive 2004/107/EC of the European Parliament and of the Council of 15 December 2004 relating to arsenic, cadmium, mercury, nickel and polycyclic aromatic hydrocarbons in ambient air. Off. Jour. Eur. Commun. L 23, 26.1.2005, p. 3–16,

[6] EU Directive 2002/95/EC, Restriction of Hazardous Substances in Electrical and Electronic Equipment, (RoHS directive 2002), www.broadcom.com/docs/ & www.chem.agilent.com/

[7] Y. N. Mikhailoskii, G. A. Berdzenishvili, Activating and passivating properties of oxygen containing anions in the corrosion processes of aluminium. Prot. Met. 22 (1986) 669-703.

[8] M. S. Vukasovich, F. J. Sullivan, Evaluation of Molybdate as an Inhibitor in Automotive Engine Coolants, Mater. Perform. 29 (1990) 25-33.

[9] A. Kh. Bairamov, S. Ch. Verdiev Oxidising type inhibitors for protection of aluminium and steel surfaces in sodium chloride solutions, Brit. Corros. Jour. 27 (1992) 128–134.

[10] C. M. Mustafa, S. M. Islam Dulal, Molybdate and Nitrite as Corrosion Inhibitors for Copper-Coupled Steel in Simulated Cooling Water, Corrosion 52 (1996) 16–22.

[11] B. R. W. Hinton, D. R. Arnott, N. E. Ryan, The inhibition of aluminium corrosion by cerium cations, Metals Forum 7 (1984) 211-217.

[12] B. R. W. Hinton, D. R. Arnott, N. E. Ryan, Cerium conversion coating for the corrosion protection of aluminium, Metals Forum 9 (1986) 162-173.

[13] B. R. W. Hinton, Review on corrosion inhibitor science and technology, in A. R. P. L. ed. Corrosion/89 symposium, NACE, pp. I-11, (1993) p. 1.

[14] L. Wilson, B. R. W. Hinton, Australian patent P10649 March 1987.

[15] M. Dabalà, L. Armelao, A. Buchbergea, I. Calliari, Cerium-based conversion layers on aluminum alloys, Appl. Surf. Sci. 172 (2001) 312–322.

[16] P. Campestrini, H. Terryn, A. Hovestad, J. H. W. de Wit, Formation of a cerium-based conversion coating on AA2024: relationship with the microstructure, Surf. Coat. Technol. 176 (2004) 365–381.

[17] B. Y. Johnson, J. Edington, M. J. O'Keefe, Effect of coating parameters on the microstructure of cerium oxide conversion coatings, Mater. Sci. Eng. A361 (2003) 225–231.

[18] B. F. Rivera, B. Y. Johnson, M. J. O'Keefe, W. G. Fahrenholtz, Deposition and characterization of cerium oxide conversion coatings on aluminum alloy 7075-T6, Surf. Coat. Technol. 176 (2004) 349–356.

[19] A. Decroly, J. P. Petitjean, Study of the deposition of cerium oxide by conversion on to aluminium alloys, Surf. Coat. Technol. 194 (2005) 1–9.

[20] D. K. Heller, W. G. Fahrenholtz, M. J. O'Keefe, The effect of post-treatment time and temperature on cerium-based conversion coatings on Al 2024-T3, Corros. Sci. 52 (2010) 360-368.

[21] J. Creus, F. Brezault, C. Rebere, M. Gadouleau, Synthesis and characterisation of thin cerium oxide coatings elaborated by cathodic electrolytic deposition on steel substrate, Surf. Coat. Technol. 200 (2006) 4636-4645.

[22] Y. Hamaoui, F. Pedraza, C. Remazeiles, S. Cohendoz, C. Perebe, L. Tifouti, J. Creus, Cathodic electrodeposition of cerium-based oxides on carbon steel from concentrated cerium nitrate solutions. Part. I. Electrochemical and analytical characterization, Mater. Chem. Phys. 113 (2009) 650-657.

[23] S. Berna, F. J. Botana, J. J. Calvino, M. Marcos, J. A. Perez-Omil, H. Vidal, Lantanide salts as alternative coirrosion inhibitors, J. Alloys Comp. 225 (1995) 638-641.

[24] M. Balasubramanian, C. A. Melendres, A. N. Mansour, X-ray absorption study of the local structure of cerium in electrochemically deposited thin films, Thin Solid Films 347 (1999) 178–183.

[25] L. Arurault, P. Monsang, J. Salley, R. S. Bes, Electrochemical preparation of adherent ceria coatings on ferritic stainless steel, Thin Solid Films, 446 (2004) 75-80.

[26] P. Stefanov, G. Atanasova, D. Stoychev, Ts. Marinova, Electrochemical deposition of CeO2 on ZrO_2 and Al_2O_3 thin films formed on stainless steel, Surf. Coat. Technol. 180/181 (2004) 446–449.

[27] C. M. Rangel, T. I. Paiva, P. P. da Luz, Conversion coating growth on 2024-T3 Al alloy The effect of pre-treatments, Surf. Coat. Technol. 202 (2008) 3369–3402.

[28] S. Seal, S. K. Bose, S. K. Roy, Improvement in the oxidation behavior of austenitic stainless steels by superficially applied cerium oxide coatings, Oxidation of Metals, 41 (1994) 139-178.

[29] C. Wang, F. Jiang, F. Wang, The characterization and corrosion resistance of cerium chemical conversion coatings for 304 stainless steel, Corros. Sci. 46 (2004) 75-89.

[30] K. Aramaki, Treatment of zinc surface with cerium(III) nitrate to prevent zinc corrosion in aerated 0.5 M NaCl, Corros. Sci. 43 (2001) 2201–2215.

[31] M. G. S. Ferreira, R. G. Duarte, M. F. Montemor, A. M. Simoes, Silanes and rare earth salts as chromate replacers for pre-treatments on galvanised steel, Electrochim. Acta, 49 (2004) 2927–2935.

[32] A. Amedeh, B. Pehlevani, S. Heshmati-Manesh, Effects of rare earth metal addition on surface morphology and corrosion resistance of hot-dipped zinc coatings, Corros. Sci. 44 (2004) 2321-2331.

[33] C. Motte, N. Maury, M-G. Olivier, J-P. Petitjean, J-F. Willem, Cerium treatments for temporary protection of electroplated steel, Surf. Coat. Technol. 200 (2005) 2366–2375.

[34] Y. Kobayashi, Y. Fujiwara, Effect of SO_4^{2-} on the corrosion behavior of cerium-based conversion coatings on galvanized steel. Electrochim. Acta, 51 (2006) 4236–4242.

[35] M. Hosseini, H. Ashassi-Sorkhabi, H. A. Y. Ghisvand, Corrosion protection of electro-galvanized steel by green conversion coatings, Jour. Rare-Earths 25 (2007) 537–543.

[36] M. Dabala, K. Brunelly, E. Napolitani, M. Margini, Cerium-based chemical conversion coating on AZ63 magnesium alloy, Surf. Coat. Technol. 172 (2003) 227-232.

[37] B. Bouchaud, J. Balmain, G. Bonnet, F. Pedraza, Correlations between electrochemical mechanisms and growth of ceria-based coatings onto nickel substrates.Electrochim. Acta 88 (2013) 98–806.

[38] I. Zhitomirsky, A. Petric, Electrochemical deposition of ceria and doped ceria films, Ceram. Internat. 27 (2001) 149–155.

[39] J. Xu, S. S. Xin, P. H. Han, R. Y. Ma, M. C. Li, Cerium chemical conversion coatings for corrosion protection of stainless steels in hot seawater environments, Mater. Corros. 64, 7 (2013) 619–624

[40] C. Wang, F. Wang, The characterization and corrosion resistance of cerium chemical conversion coatings for 304 stainless steel, Corros. Sci. 46, 1, (2004) 75-89

[41] M. R. Majdi, I. Danaee, S. S. Afghahi, Preparation and Anti-Corrosive Properties of Cerium Oxide Conversion Coatings on Steel X52, Mater. Res. 20, 2 (2017) 445-451

[42] J. Creus, F. Brezault, C. Rebere, M. Gadouleau, Synthesis and characterisation of thin cerium oxide coatings elaborated by cathodic electrolytic deposition on steel substrate, Surf. Coat. Technol. 200 (2006) 4636–4645

[43] B.Ramezanzadeh, H.Vakili.R.Amini, Improved performance of cerium conversion coatings on steel with zinc phosphate post-treatment, J. Ind. Eng. Chem. 30 (2015) 225 - 233

[44] H. Hasannejad, T. Shahrabi, M. Jafarian, Synthesis and properties of high corrosion resistant Ni–cerium oxide nano-composite coating, Mater. Corros. 64, 12 (2013) 1104–1113

[45] X. Jiang, R. Guo, S. Jiang, Evaluation of self-healing ability of Ce–V conversion coating on AZ31 magnesium alloy. J. Magnes. Alloys, 4, (2016) 230–241

[46] A. J. Davenport, H. S. Isaacs, M. W. Kendig, X-Ray Absorption Study of Cerium in the Passive Film on Aluminum, J. Electrochem. Soc. 136 (1989) 1837-1838.

[47] J. O. Stoffer, T. J. O'Keefe, E. Morris, S. A. Hayes, P. Yu, A. Williams, X. Lin, US Patent No 2004 /0026260 A1

[48] W. G. Fahrenholz, M. J. O'Keefe, H. Zhou, J. T. Grant, Characterization of cerium-based conversion coatings for corrosion protection of aluminum alloys, Surf. Coat. Technol. 155 (2002) 208-213.

[49] Y. Xingwen, C. Chunan, Y. Zhiming, Z. Derui, Y. Zhongda, Study of double layer rare earth metal conversion coating on aluminum alloy LY12, Corros. Sci. 43 (2001) 1283-1294.

[50] S. Kozhukharov, J. A. P. Ayuso, D. S. Rodríguez, O. F. Acuña, M. Machkova, V. Kozhukharov Optimization of the basic parameters of cathodic deposition of Ce-conversion coatings on D16 AM clad alloy, J. Chem. Technol. Metall. 48 (2013) 296-307.

[51] K. Brunelli, F. Bisaglia, J. Kovac, M. Magrini, M. Dabala, Effects of cathodic electrodeposition parameters of cerium oxide film on the corrosion resistance of the 2024 Al alloy, Mater. Corros. 7 (2009) 514–520.

[52] L. J. Zivkovic, J. P. Popic, B. V. Jegdic, Z. Dohcevic-Mitrovic, J. B. Bajat, V. B. Miskovic-Stankovic, Corrosion study of ceria coatings on AA6060 aluminium alloy obtained by

cathodic electrodeposition: Effect of deposition potential, Surf. Coat. Technol. 240 (2014) 327–335.

[53] Y. Zhou, J. A. Switzer, Growth of cerium (IV) oxide films by the electrochemical generation of base method, J. Alloys Comp. 237 (1996) 1-5.

[54] I. Zhitomirsky, A. Petric, Electrolytic and electrophoretic deposition of CeO_2 films, Mater. Lett. 40 (1999) 263– 268.

[55] J-M. Brossard, J. Baumain, J. Creus, G. Bonnet, Characterization of thin solid films containing yttrium formed by electrogeneration base for high temperature corrosion applications, Surf. Coat. Technol. 185 (2004) 275-282.

[56] A. E. Hughes, R. J. Taylor, B. R. W. Hinton, L. Wilson, XPS and SEM Characterization of Hydrated Cerium Oxide Conversion Coatings, Surf. Interface. Anal. 23 (1995) 540–550.

[57] A. J. Aldykiewicz, A. J. Davenport, H. S. Isaacs, Studies of the Formation of Cerium-Rich Protective Films Using X-Ray Absorption Near-Edge Spectroscopy and Rotating Disk Electrode Methods, J. Electrochem. Soc. 143 (1996) 147-154.

[58] P. Yu, S. A. Hayes, T. J. O'Keefe, M. J. O'Keefe, J. O. Stoffer, The phase stability of cerium species in aqueous systems II. The Ce(III)/Ce(IV) – H_2O – H_2O_2/O_2 systems. Considerations and Porbaix diagram calculations, J. Electrochem. Soc. 153(1) (2006) C74-C79.

[59] A. M. Sukhotyna, Manual of Electrochemistry, Gov. Ed. "Chemistry" (1981) St. Petersburg. p. 140.

[60] F. H. Scholes, C. Soste, A. E. Hughes, S. G. Hardin, P. R. Curtis, The role of hydrogen peroxide in the deposition of cerium-based conversion coatings, Appl. Surf. Sci. 253 (2006) 1770–1780.

[61] Arnott D R, Ryan N E, Hinton B R W, Sexton B A, Hughes A E (1985) Auger and XPS studies of cerium corrosion inhibition on 7075 aluminum alloy. Appl Surf Sci 22/23:236-251. DOI: 10.1016/0378-5963(85)90056-X

[62] F-B. Li, G. E. Thompson, In Situ Atomic Force Microscopy Studies of the Deposition of Cerium Oxide Films on Regularly Corrugated Surfaces, J. Electrochem. Soc. 146 (1999) 1809–1815.

[63] A. J. Bard, L. R. Faulkner, Electrochemical Methods. Fundamentals and Applications, 2nd Ed. Wiley, New York. (2001), p. 143. ISBN 0-471-04372-9

[64] E. A. Matter, S. Kozhukharov, M. Machkova, V. Kozhukharov, Comparison between the inhibition efficiencies of Ce(III) and Ce(IV) ammonium nitrates against corrosion of AA2024 aluminum alloy in solutions of low chloride concentration, Corros. Sci. 62 (2012) 22–33.

[65] K. Aramaki, The inhibition effects of cation inhibitors on corrosion of zinc in aerated 0.5 M NaCl, Corros. Sci. 43 (2001) 1573-1588.

[66] M. Hoang, A. E. Hughes, T. W. Turney, An XPS study of Ru-promotion for Co/CeO_2, Fischer-Tropsch catalyst, Appl. Surf. Sci. 72 (1993) 55–65.